

Error Mitigation Thresholds in Noisy Quantum Circuits

Pradeep Niroula,¹ Sarang Gopalakrishnan,² and Michael J. Gullans¹

¹*Joint Center for Quantum Information and Computer Science,
NIST/University of Maryland, College Park, Maryland 20742, USA*

²*Department of Electrical Engineering, Princeton University, Princeton, NJ 08544, USA.*

(Dated: February 10, 2023)

Extracting useful information from noisy near-term quantum simulations requires error mitigation strategies. A broad class of these strategies rely on precise characterization of the noise source. We study the performance of such strategies when the noise is imperfectly characterized. We adapt an Imry-Ma argument to predict the existence of an *error mitigation threshold* for random spatially local circuits in spatial dimensions $D \geq 2$: characterization disorder below the threshold rate allows for error mitigation up to times that scale with the number of qubits. For one-dimensional circuits, by contrast, mitigation fails at an $\mathcal{O}(1)$ time for any imperfection in the characterization of disorder. We discuss implications for tests of quantum computational advantage, fault-tolerant probes of measurement-induced phase transitions, and quantum algorithms in near-term devices.

Noise presents a fundamental barrier to realizing scalable quantum information processing [1]. The theory of fault-tolerant quantum error correction shows how this barrier can be overcome in principle [2–4]. However, despite remarkable experimental progress establishing the basic validity of the theory of fault-tolerance [5–8], achieving large-scale quantum computing with error corrected qubits remains a formidable challenge. In recent years, quantum error mitigation has emerged as a complementary paradigm for addressing the effects of noise in large-scale quantum devices [9–21]. At its core, error mitigation relies on the ability to accurately characterize the interaction of the system with its environment. Armed with this knowledge, one can design classical post-processing techniques to construct more accurate estimators of the noiseless signal using data obtained from a noisy device. Similar methods have been ubiquitously employed in quantum process tomography to reliably extract error models in the presence of noisy operations [22–24]; using these methods to improve the accuracy of noisy quantum circuits is a more recent development.

A key aspect of the threshold theorem for fault-tolerant quantum computing is that it applies even in the case where the individual components used to implement the error correction are noisy. An analogous question for error mitigation strategies is whether they work when the noise is imperfectly characterized. As noted above, related questions have been addressed for quantum process tomography in the presence of faulty operations [22–24]; however, these models are often considered only at the level of a few qubits, generally precluding the existence of a sharply defined phase transition. In the case of many-body tomographic problems (e.g., Pauli noise estimation [25, 26] or Hamiltonian learning [27, 28]), thresholds in learnability are possible and likely arise under some circumstances. However, to our knowledge, threshold results have not been considered for quantum error mitigation.

In this paper, we demonstrate the possibility of thresholds for quantum error mitigation. We focus on one of the conceptually simplest quantum error mitigation tech-

niques, which goes under the moniker “probabilistic error cancellation” (PEC) [11, 29]. PEC relies on the fact that many of the most common noise channels used to model quantum devices are actually trivially invertible at the mathematical level. Unfortunately, the inverse operation is not generally a physical evolution. For example, the inverse of the depolarizing channel violates the complete-positivity condition for quantum channels. As a result, the only known way to implement the inverse is through classical post-processing. In the case of PEC, this classical post-processing step is implemented via Monte Carlo sampling methods but, for constant noise rates, incurs exponential sampling overheads in the worst case [11, 29]. Nevertheless, PEC can be used to significantly extend the accessible circuit depths of a given noisy quantum device, as demonstrated in recent experiments [29]. Some other examples of quantum error mitigation include zero-noise extrapolation [11–13], symmetry-based error detection [15, 16], cooling/purification [17–19], and learning based methods [20, 21]. In the remainder of the paper we will focus on the PEC technique, primarily because of its conceptual simplicity.

Our central prediction is that PEC has an error mitigation threshold for random, spatially local circuits in spatial dimensions $D \geq 2$ when the noise is imperfectly characterized. Building on the extensive work characterizing quantum phases and phase transitions in hybrid random circuits [30, 31], we consider a model of random unitary circuits subject to depolarizing noise with binary disorder in the depolarization rate [see Fig. 1(a)]. To mitigate the effects of the noise we apply a uniform “antinoise” channel that inverts the depolarizing noise on average. We show that a replica statistical mechanics description of the problem has close parallels to the classical random field Ising model (RFIM) in $D + 1$ dimensions. At the zero-mean field condition in the RFIM, Imry-Ma arguments [32] show that the ordered phase survives random symmetry-breaking terms in sufficiently high dimensions. In the random circuit problem, this analysis indicates the possibility for error mitigation thresholds for $D \geq 2$, while $D = 1$ is the marginal dimension. We also ana-

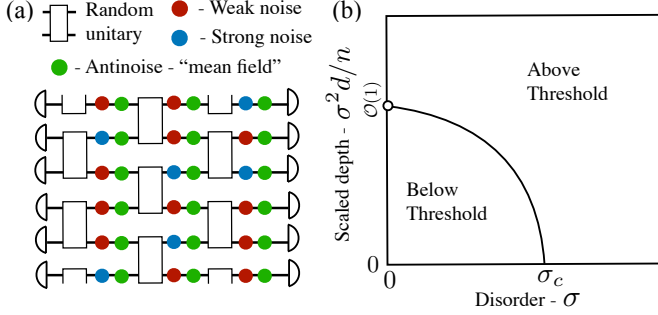


FIG. 1. Model and phase diagram: (a) Noisy random circuit with spacetime disorder in the noise rate and error mitigation. (b) Phase diagram for the error mitigation threshold in this model for $D \geq 2$ spatial dimensions. At high disorder rates and linear depths, the system transitions from a “below-threshold” phase where mitigation succeeds on average to an “above-threshold” phase where mitigation fails.

lyze the performance of error mitigation as a function of circuit depth. For depths larger than the linear size of the system, the mitigation fails, resulting in a signal worse than that obtained by sampling from the uniform distribution. The corresponding phase diagram of the system is shown in Fig. 1(b) for $D \geq 2$. Analytic and numerical studies of the two-copy replica theory and exact simulations of the mitigated circuit dynamics confirm our predictions.

Model and Simplified Limits.—The basic model we consider in this work is illustrated in Fig. 1(a). Each two-site gate is chosen to be Haar random [33–35] and are interspersed with noise and antinoise channels. We focus on the case of depolarizing noise and its inverse channel as the antinoise

$$\mathcal{E}_{\mathbf{x},t}(\rho) = (1 - q_{\mathbf{x},t})\rho + q_{\mathbf{x},t} \text{tr}_{\mathbf{x}}[\rho] \otimes I/2, \quad (1)$$

$$\mathcal{A}_{\mathbf{x}}(\rho) = \frac{\rho - q_a \text{tr}_{\mathbf{x}}[\rho] \otimes I/2}{1 - q_a}, \quad (2)$$

where $\text{tr}_{\mathbf{x}}[\rho]$ is a partial trace operation at site \mathbf{x} . Tuning $q_a = q_{\mathbf{x},t}$ inverts the noise at space-time site (\mathbf{x}, t) such that $\mathcal{A}_{\mathbf{x}} \circ \mathcal{E}_{\mathbf{x},t}(\rho) = \rho$. To include the disorder, the noise rates are drawn randomly at each space-time location of the circuit from one of two values $q_{\mathbf{x},t} = q_{1/2}$ with probability $p/1 - p$ and $q_1 < q_2$. The antinoise can be tuned to a zero mean-field condition by taking $(1 - q_a) = (1 - q_1)^p(1 - q_2)^{1-p}$ equal to a geometric mean. This condition ensures that a Pauli operator $\sigma_{\mathbf{x}}^{\mu}$ ($\mu \in \{X, Y, Z\}$) evolved under multiple rounds of noise and antinoise up to depth $t = d$ will have expectation value

$$\text{tr} \left[\sigma_{\mathbf{x}}^{\mu} \prod_{t=1}^d \mathcal{A}_{\mathbf{x}} \circ \mathcal{E}_{\mathbf{x},t}(\rho) \right] = \prod_t \frac{1 - q_{\mathbf{x},t}}{1 - q_a} \text{tr}[\sigma_{\mathbf{x}}^{\mu} \rho], \quad (3)$$

where the prefactor tends to a log-normal distribution that concentrates around one. Any deviations of q_a from

this zero mean-field condition will result in an exponential growth rate that scales linearly in the depth d . At the zero-mean field condition, however, the noise is canceled on average and the prefactor deviates from one only due to random fluctuations as $e^{\pm \mathcal{O}(\sqrt{d})}$ (i.e., the exponential growth rate is suppressed by a factor \sqrt{d}).

To develop some basic intuition for how unitary dynamics can improve the robustness of error mitigation, it is helpful to consider a toy model consisting of two sites L/R with $q_L < q_R$ fixed in time. Now, take $1 - q_a = \sqrt{(1 - q_R)(1 - q_L)}$ to satisfy the zero mean-field condition. The R site will be subject to excess noise and the L site will experience excess antinoise. The case of weak unitary dynamics is analogous to the above threshold phase. In the limit where the unitary dynamics tends to trivial evolution, any state initialized with non-zero Pauli expectation value on site L will experience exponential growth of the expectation values leading to an unphysical density matrix after an $\mathcal{O}(1)$ time. We discuss below how this type of rapid instability to unphysical states is characteristic of the above threshold phase.

To build in the effects of unitary dynamics, consider the base circuit to consist of repeated applications of SWAP gates. In this case, it is readily verified that the effects of the noise on Pauli expectation values will be completely canceled for arbitrarily deep circuits except for the most recent layer of gates. In this two-qubit example, Haar random gates behaves similarly to SWAP gates in that the noise is cancelled on average. However, the temporal randomness will lead to exponential fluctuations of Pauli expectation values of size $e^{\mathcal{O}(\sqrt{d})}$, where the term in the exponent will follow the statistics of a random walk. This tendency of the random unitary dynamics to suppress effects of the noise/antinoise from linear in d to \sqrt{d} scaling for certain initial conditions is characteristic of the behavior we find for the below-threshold phase. To more quantitatively capture the trends found in this simple two-site model, we now develop a mean-field theory for the threshold.

Mean-field theory.—In deriving a mean-field theory, it is convenient to turn to a more analytically tractable model formulated in continuous time rather than as a discrete circuit. The noise and antinoise are now captured through a Lindblad master equation [36]

$$\dot{\rho} = -i[H(t), \rho] - \sum_j (\gamma_j - \gamma_a)(\rho - \text{tr}_j[\rho] \otimes I/2), \quad (4)$$

$$H(t) = \sum_{i < j, \mu, \nu} J_{ij\mu\nu}(t) \sigma_i^{\mu} \sigma_j^{\nu}, \quad (5)$$

where $H(t)$ is a time-dependent Hamiltonian that sets the unitary evolution, γ_i is the random noise rate on site i , and γ_a is the antinoise rate. The noise rate $\gamma_i = \gamma_{1/2}$ is drawn randomly with probability $p/1 - p$. The zero mean-field condition becomes $\gamma_a = \bar{\gamma} \equiv p \gamma_1 + (1 - p) \gamma_2$. We take the random unitary dynamics to be given by an all-to-all coupled Brownian circuit model in which the

$J_{ij\mu\nu}(t)$ are drawn from a white-noise Gaussian random process with variance parameters [37, 38]

$$\langle J_{ij\mu\nu}(t) J_{k\ell\gamma\delta}(t') \rangle = \frac{J}{2N} \delta_{ik} \delta_{j\ell} \delta_{\mu\gamma} \delta_{\nu\delta} \delta(t - t'). \quad (6)$$

To treat this model analytically, we average the dynamics over the random coupling constants for multiple identical copies of the density matrix $\rho(t)^{\otimes k}$ (k is a replica index). In the equations of motion for the averaged moments $\rho_k(t) \equiv \mathbb{E}_H[\rho^{\otimes k}]$, the unitary drive-term averages to zero, leading to a purely dissipative master equation for $\rho_k(t)$ (see Appendix A). Focusing on second moments ($k = 2$) gives rise to a particularly simple model where with two global steady states given by $I^{\otimes N}$ and $S^{\otimes N}$ [38], where S is the SWAP operator acting on the two copies. The all SWAP steady-state captures non-trivial corrections to second moment observables like the purity of sub-systems. In the mean-field approximation, we enforce the density matrix to take a product state form $\rho_2 = \bigotimes_{i=1}^N \sigma_i$. Due to the lack of symmetries or conservation laws in the problem, σ_i can be parameterized as

$$\sigma_i = (1/4 + \delta_i)|s\rangle\langle s| + (1/4 - \delta_i/3)P_T, \quad (7)$$

where δ_i is the deviation from an infinite temperature state, $|s\rangle$ is a two-qubit singlet state across the two copies, and P_T is the projector onto the two-qubit triplet subspace of the two copies.

The mean-field equations for δ_i take the form

$$\dot{\delta}_i = -4 \left[\Delta_i + \frac{J}{N} \sum_{j \neq i} (3 + 4\delta_j) \right] \delta_i, \quad (8)$$

where $\Delta_i = \gamma_i - \gamma_a$. This simple equation captures much of the basic physics we described in the two-site model, while also exhibiting the phase transition. Notably, we can see that at weak values of the disorder, the interaction term acts as a restoring force towards the fixed point $\delta_i = 0$. The other fixed point $\delta_i = -3/4$ corresponds to an unphysical density matrix, which is unstable at weak disorder. At a critical disorder strength of $|\Delta_1| = 3J$ (see App. A), however, the $\delta_i = 0$ fixed point becomes unstable. The dynamics flows to a new stable fixed point which is an unphysical density matrix. Thus, we see that the above threshold phase in the mean-field theory is characterized by an instability of the density matrix to unphysical states.

To rigorously characterize the threshold behavior, particularly in finite-dimensional systems, we need a more systematic treatment of the correlations in the state beyond the mean-field approximation. To develop this approach, it is convenient to return to the circuit models. In these discrete models, the connections to the physics of the RFIM become more explicit.

Statistical Mechanics Mapping.—Our rigorous analysis of the problem relies on well-established mappings from

random quantum circuit dynamics in D spatial dimensions to statistical mechanics models in $D + 1$ dimensions [34, 35, 39–44]. We outline the details of the mapping in Appendix B. The approach we take is to expand $\rho_k \equiv \mathbb{U}[\rho^{\otimes k}]$ into a basis of operators based on representations of the permutation group S_k [41]. One can then derive update rules for the averaged state following each layer of gates, noise, and antinoise. In this paper, we focus on the two-replica case where the two operators are I and S (the SWAP gate). We expect this model to be sufficient to capture many of the properties of the transition, as has been argued in the unitary case [34]. Numerical evidence based on exact simulations is presented below that support this claim.

Without noise/antinoise, ρ_2 has two fixed points $I^{\otimes N}$ and $S^{\otimes N}$ just as in the Brownian circuit model. Configurations with persistent “domain walls” (i.e., mixtures of I and S) are exponentially damped with depth in the model. As a result, the two fixed points can be interpreted as ferromagnetic ground states of an Ising-type spin model. In this interpretation, noise acts as a symmetry breaking field because it favors the identity configuration and damps out configurations with S operators [40]. antinoise acts as a field in the opposite direction, but it also adds additional sign-structure to the problem from the second term in Eq. (2). We account for this sign by labeling spacetime configurations of I and S operators by the sign of their contribution, then we can write $\rho_2 = \rho_2^+ - \rho_2^-$, where ρ_2^\pm sum over spacetime configurations with a positive/negative sign.

Imry-Ma arguments.—To make precise connections to Imry-Ma arguments [32], we rigorously analyze finite-dimensional versions of the statistical mechanics models. First, we define a *simple initial condition* as a state ρ_2 that is identity everywhere except in a contiguous region A where it is given by $\text{tr}_{A^c}[\rho_2] \propto I^{\otimes |A|} + S^{\otimes |A|}$. Such an initial condition can be prepared physically by taking a Haar random state (or a state drawn from a two-design such as the Clifford group [45]) on A and the infinite temperature state on the complement of A . The first model we consider is a *quenched 1D* model described by a one-dimensional brickwork circuit of the type shown in Fig. 1(a) with Haar random two-qubit gates and spatially random noise rates that are constant in time. We define $\sigma = \sqrt{p(1-p)(q_2 - q_1)}$ as the standard deviation of the noise rates. We prove that the quenched 1D model always exhibits an instability for one of the simple initial conditions.

Theorem 1 (Instability in quenched 1D). For the quenched 1D model with any $\sigma > 0$, there is a simple initial condition for subregion A of size $\mathcal{O}(\log N)$ such that as $N \rightarrow \infty$ and $d \rightarrow \infty$ with high probability $\|\rho_2^\pm\| \geq e^{\mathcal{O}(d \log N)} / 2^{2N-|A|} 3^{|A|}$.

Proof. The proof of the theorem essentially follows a standard Imry-Ma argument. For any finite σ as $N \rightarrow \infty$ with high probability (whp) there will be a contiguous region of sites A with noise rate q_1 of size $|A| = \mathcal{O}(\log N)$.

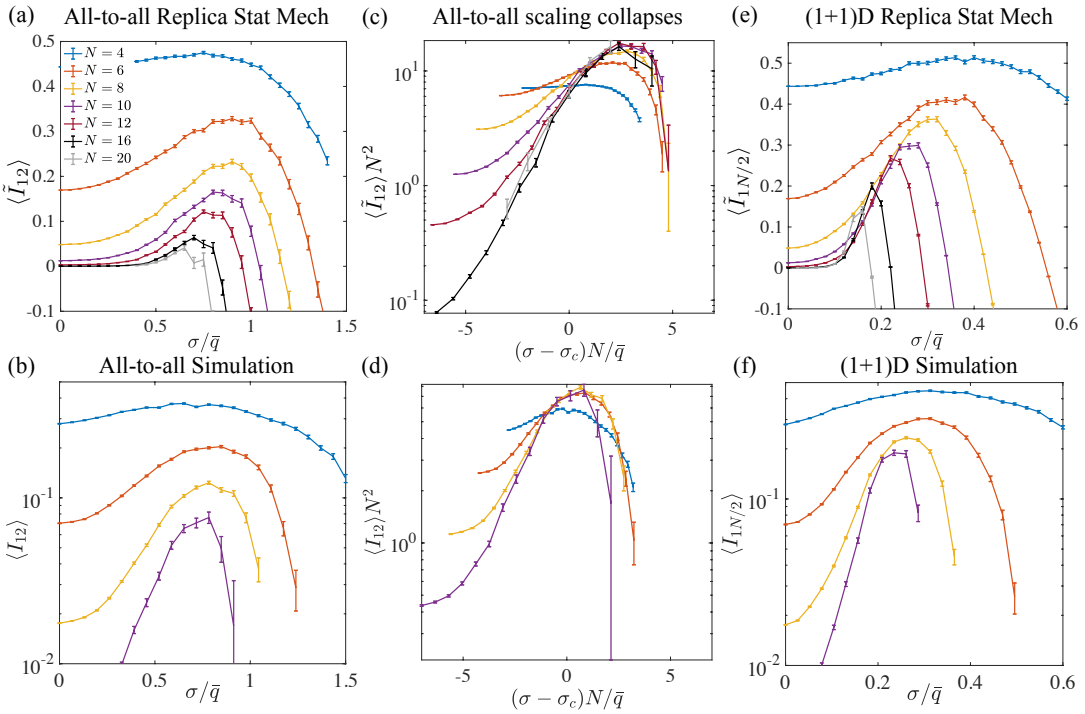


FIG. 2. Numerical tests of the threshold theory: (a) Numerical simulations of circuit and noise-disorder averaged the correlation metric \tilde{I}_{12} obtained from purity of subregions for two random sites in the system. (b) Mutual information I_{12} for exact simulations of the mitigated noisy random circuit. (c-b) Scaling collapse of data from (a-b) using $\sigma_c/\bar{q} = 0.65(5)/0.55(5)$ and critical exponent on x -axis obtained from local probe (see Appendix C). The critical scaling on the y -axis is an ansatz. (e-f) Similar quantities as (a-b) for antipodal sites of a 1D chain. The strong drift in the peak with increasing system size is consistent with the lack of a below-threshold phase in this model.

For sufficiently large N there will be a region satisfying $(1 - q_1)^{|A|}/(1 - q_a)^{|A|} > (5/2)^2$ whp, which implies that the $\mathcal{O}(1)$ boundary cost of the two domain walls at the edge of A can be overcome by the amplification of the S configurations in the bulk. Taking a configuration of all S on A with identities elsewhere that moves by order 1 site at the boundary at each time-step according to the rules for the replica model provides a contribution to ρ_2^\pm that diverges as $e^{\mathcal{O}(d \log N)}/2^{2N-|A|}3^{|A|}$. The denominator is the normalization constant for the initial state. \square

As a corollary to this result, an initial pure product state evolved with this model will also have this instability. The converse of this type of Imry-Ma argument is that we expect the instability of these initial conditions to be suppressed for weak enough disorder for high enough dimensions. In this case, for large regions A the boundary cost of the domain wall scales as $|A|^{(D-1)/D}$, whereas the amplification from the antinoise scales as $|A|^{1/2}$. As a result, with quenched disorder in time, we expect the instability to vanish for $D \geq 3$ at sufficiently small values of σ , while $D = 2$ is the marginal dimension. For space-time random disorder, the marginal dimension is $D = 1$ and an ordered phase persists for $D \geq 2$. Note, that at large values of σ , the domain wall cost can be overcome even by a single site with strong antinoise, leading to

an instability. As a result, there will be a disorder driven phase transition at finite σ in sufficiently high-dimensions associated with the onset of this instability.

Numerical Tests.—Figure 2 summarizes our numerical results. We run numerical simulations of random circuits, together with noise and antinoise, to characterize this phase transition in two settings. In the first case [see Fig. 2(a-d)], we simulate an infinite-dimensional circuit where entangling gates can exist between any pair of qubits and noise is random in both space and time. In the second case [see Fig. 2(e-f)], we simulate $(1+1)D$ circuit dynamics assuming quenched noise, where the randomness is only spatial. The first model is a test of the high-dimensional limit of the model, while the second model is the same one considered in Theorem 1.

In both cases, we initialize a state of a N -qubit register in a global Haar-random state, which corresponds to the string $\propto I^{\otimes N} + S^{\otimes N}$ in the statistical-mechanical mapping. For the infinite-dimension model, we apply random Haar gates on a set of $N/2$ disjoint pairs, randomly drawn from all $N(N-1)/2$ possible pairs of qubits. For the $(1+1)D$ model, each time-step corresponds to a layer in the brickwork circuit in Fig. 1 with periodic boundary conditions. Each layer of unitary gates is followed by the noise-antinoise channel on all qubits.

After evolving the circuit to depth d , we take the partial trace of two qubits and calculate correlation metrics between the two qubits [46, 47]. These low-order correlations are exponentially suppressed in N for $\sigma = 0$, but they develop a peak at the critical point where long-range correlations develop. For $D = 1$, the pair consists a randomly chosen qubit and its corresponding anti-pode at a distance of $N/2$; for the all-to-all model, both qubits are randomly chosen.

We study the two systems using the replica statistical-mechanical mapping introduced above, with background details in B. The mapping lets us probe the phase transition for system sizes as large as $N = 20$. For sizes up to $N = 10$, we complement the numerics on statistical-mechanical mapping with direct circuit simulations. In the replica stat-mech model we study a measure of correlations $\tilde{I}_{ab} = -\log_2 \mathbb{E}_U[\text{Tr}[\rho_a^2]] - \log_2 \mathbb{E}_U[\text{Tr}[\rho_b^2]] + \log_2 \mathbb{E}_U[\text{Tr}[\rho_{ab}^2]]$ averaged over noise-disorder (denoted by $\langle \cdot \rangle$ brackets), while in the exact simulations we study the standard mutual information $I_{ab} = S_a + S_b - S_{ab}$ for the von Neumann entropy $S_a = -\text{tr}[\rho_a \log_2 \rho_a]$ [1].

The numerical results provide strong supporting evidence for the theoretical scenario outlined above. We see evidence for a stable ordered phase in the high-dimensional limit of the all-to-all model, whereas the 1D model with quenched randomness in the noise is consistent with the lack of an ordered phase. In addition, we estimate critical exponents for the transition in Fig. 2(b-c) that are consistent with simple rational values characteristic of mean-field behavior.

Outlook.—An important application of our results is to improved benchmarking and verification of random circuit sampling in noisy devices [48–53]. In Appendix D, we demonstrate an exponential improvement in a mitigated version of the so-called “linear cross-entropy” fidelity below the error mitigation threshold. Notably, this mitigated benchmark can be computed using existing experimental data. The below threshold behavior may have important consequences for proofs of quantum computational advantage in noisy circuits [43, 54, 55], potentially motivating the inclusion of error mitigation in complexity theoretic arguments. Moreover, the exponential im-

provement in the fidelity score for $D \geq 2$ might indicate a method to foil “spoofing” algorithms that have been developed for unmitigated fidelity benchmarks in noisy random circuits [44].

These results also have implications for measurement-induced phase transitions in hybrid random circuits [30, 31, 46, 47]. Such models are not fault-tolerant because circuit-level depolarizing noise drives the system to a short-range correlated mixed state (it acts as a symmetry breaking field in the replica theory [40]). The addition of the antinoise terms considered here can restore the symmetries of the model on average, allowing for a stable ordered phase. Thus, our analysis indicates that MIPT for $D \geq 2$ can be made fault-tolerant via error mitigation techniques.

More broadly, the existence of error mitigation thresholds has important implications for near-term quantum simulation and quantum computing. A natural question is whether the threshold behavior observed here extends to other models. For example, in quantum simulation of Hamiltonian dynamics, one can apply a continuous time version of PEC [36]. An error mitigation threshold qualitatively similar to the one studied in this work should arise for chaotic Hamiltonian evolution with sufficiently strong interactions relative to the dissipation, raising the intriguing possibility of a rich interplay between the Hamiltonian and error mitigated dynamics. Similarly, error mitigation thresholds may naturally arise in more conventional quantum algorithms like Shor’s factoring algorithm.

ACKNOWLEDGMENTS

We thank Chris Baldwin, Gregory Bentsen, Abhinav Deshpande, Bill Fefferman, Alexey Gorshkov, David Huse, Zlatko Minev, Alireza Seif, Sagar Vijay, and Brayden Ware for helpful discussions. Work supported in part by NSF QLCI grant OMA-2120757, by NSF DMR-1653271, and NSF grant PHY-1748958.

[1] M. A. Nielsen and I. L. Chuang, *Quantum Computation and Quantum Information*, 10th ed. (Cambridge University Press, New York, NY, USA, 2011).

[2] D. Aharonov and M. Ben-Or, in *Proceedings of the Twenty-Ninth Annual ACM Symposium on Theory of Computing - STOC ’97* (ACM Press, El Paso, Texas, United States, 1997) pp. 176–188.

[3] E. Dennis, A. Kitaev, A. Landahl, and J. Preskill, *J. Math. Phys.* **43**, 4452 (2002).

[4] D. Gottesman, (2009), arXiv:0904.2557.

[5] L. Egan, D. M. Debroy, C. Noel, A. Risinger, D. Zhu, D. Biswas, M. Newman, M. Li, K. R. Brown, M. Cetina, and C. Monroe, *Nature* **598**, 281 (2021).

[6] S. Krinner, N. Lacroix, A. Remm, A. D. Paolo, E. Genois, C. Leroux, C. Hellings, S. Lazar, F. Swiadek, J. Hermann, G. J. Norris, C. K. Andersen, M. Müller, A. Blais, C. Eichler, and A. Wallraff, *Nature* **605**, 669 (2022), 2112.03708.

[7] R. Acharya, I. Aleiner, R. Allen, T. I. Andersen, M. Ansmann, F. Arute, K. Arya, A. Asfaw, J. Atalaya, R. Babbush, D. Bacon, J. C. Bardin, J. Basso, A. Bengtsson, S. Boixo, G. Bortoli, A. Bourassa, J. Bovaird, L. Brill, M. Broughton, B. B. Buckley, D. A. Buell, T. Burger, B. Burkett, N. Bushnell, Y. Chen, Z. Chen, B. Chiaro, J. Cogan, R. Collins, P. Conner, W. Courtney, A. L. Crook, B. Curtin, D. M. Debroy, A. D. T. Barba, S. Demura, A. Dunsworth, D. Eppens, C. Erickson, L. Faoro, E. Farhi, R. Fatemi, L. F. Burgos,

E. Forati, A. G. Fowler, B. Foxen, W. Giang, C. Gidney, D. Gilboa, M. Giustina, A. G. Dau, J. A. Gross, S. Habegger, M. C. Hamilton, M. P. Harrigan, S. D. Harrington, O. Higgott, J. Hilton, M. Hoffmann, S. Hong, T. Huang, A. Huff, W. J. Huggins, L. B. Ioffe, S. V. Isakov, J. Iveland, E. Jeffrey, Z. Jiang, C. Jones, P. Juhas, D. Kafri, K. Kechedzhi, J. Kelly, T. Khattar, M. Khezri, M. Kieferová, S. Kim, A. Kitaev, P. V. Klimov, A. R. Klots, A. N. Korotkov, F. Kostritsa, J. M. Kreikebaum, D. Landhuis, P. Laptev, K.-M. Lau, L. Laws, J. Lee, K. Lee, B. J. Lester, A. Lill, W. Liu, A. Locharla, E. Lucero, F. D. Malone, J. Marshall, O. Martin, J. R. McClean, T. McCourt, M. McEwen, A. Megrant, B. M. Costa, X. Mi, K. C. Miao, M. Mohseni, S. Montazeri, A. Morvan, E. Mount, W. Mruczkiewicz, O. Naaman, M. Neeley, C. Neill, A. Nersisyan, H. Neven, M. Newman, J. H. Ng, A. Nguyen, M. Nguyen, M. Y. Niu, T. E. O'Brien, A. Opremcak, J. Platt, A. Petukhov, R. Potter, L. P. Pryadko, C. Quintana, P. Roushan, N. C. Rubin, N. Saei, D. Sank, K. Sankaragomathi, K. J. Satzinger, H. F. Schurkus, C. Schuster, M. J. Shearn, A. Shorter, V. Shvarts, J. Skrzyn, V. Smelyanskiy, W. C. Smith, G. Sterling, D. Strain, M. Szalay, A. Torres, G. Vidal, B. Villalonga, C. V. Heidweiller, T. White, C. Xing, Z. J. Yao, P. Yeh, J. Yoo, G. Young, A. Zalcman, Y. Zhang, and N. Zhu, arXiv:2207.06431 (2022), 10.48550/ARXIV.2207.06431.

[8] V. V. Sivak, A. Eickbusch, B. Royer, S. Singh, I. Tsioris, S. Ganjam, A. Miano, B. L. Brock, A. Z. Ding, L. Frunzio, S. M. Girvin, R. J. Schoelkopf, and M. H. Devoret, arXiv (2022), 10.48550/arxiv.2211.09116.

[9] S. McArdle, S. Endo, A. Aspuru-Guzik, S. C. Benjamin, and X. Yuan, Rev. Mod. Phys. **92**, 015003 (2020).

[10] Z. Cai, R. Babbush, S. C. Benjamin, S. Endo, W. J. Huggins, Y. Li, J. R. McClean, and T. E. O'Brien, arXiv preprint arXiv:2210.00921 (2022).

[11] K. Temme, S. Bravyi, and J. M. Gambetta, Phys. Rev. Lett. **119**, 180509 (2017).

[12] Y. Li and S. C. Benjamin, Phys. Rev. X **7**, 021050 (2017).

[13] Y. Kim, C. J. Wood, T. J. Yoder, S. T. Merkel, J. M. Gambetta, K. Temme, and A. Kandala, Nature Phys. (2023), 10.1038/s41567-022-01914-3.

[14] J. R. McClean, M. E. Kimchi-Schwartz, J. Carter, and W. A. de Jong, Phys. Rev. A **95**, 042308 (2017).

[15] X. Bonet-Monroig, R. Sagastizabal, M. Singh, and T. E. O'Brien, Phys. Rev. A **98**, 062339 (2018).

[16] S. McArdle, X. Yuan, and S. Benjamin, Phys. Rev. Lett. **122**, 180501 (2019).

[17] J. Cotler, S. Choi, A. Lukin, H. Gharibyan, T. Grover, M. E. Tai, M. Rispoli, R. Schittko, P. M. Preiss, A. M. Kaufman, M. Greiner, H. Pichler, and P. Hayden, Phys. Rev. X **9**, 031013 (2019).

[18] W. J. Huggins, S. McArdle, T. E. O'Brien, J. Lee, N. C. Rubin, S. Boixo, K. B. Whaley, R. Babbush, and J. R. McClean, Phys. Rev. X **11**, 041036 (2021).

[19] B. Koczor, Phys. Rev. X **11**, 031057 (2021).

[20] P. Czarnik, A. Arrasmith, P. J. Coles, and L. Cincio, Quantum **5**, 592 (2021).

[21] A. Strikis, D. Qin, Y. Chen, S. C. Benjamin, and Y. Li, PRX Quantum **2**, 040330 (2021).

[22] J. Emerson, R. Alicki, and K. Źyczkowski, J Opt. B Quantum Semiclassical Opt. **7**, S347 (2005).

[23] E. Knill, D. Leibfried, R. Reichle, J. Britton, R. B. Blakestad, J. D. Jost, C. Langer, R. Ozeri, S. Seidelin, and D. J. Wineland, Phys. Rev. A **77**, 012307 (2008).

[24] E. Nielsen, J. K. Gamble, K. Rudinger, T. Scholten, K. Young, and R. Blume-Kohout, Quantum **5**, 557 (2021).

[25] S. T. Flammia and J. J. Wallman, ACM Transactions on Quantum Computing **1** (1), 1-32 (2020). arXiv:1907.12976.

[26] R. Harper, S. T. Flammia, and J. J. Wallman, Nature Physics **332**, 1059 (2020).

[27] E. Bairey, I. Arad, and N. H. Lindner, Physical Review Letters **122**, 020504 (2019).

[28] A. Anshu, S. Arunachalam, T. Kuwahara, and M. Soleimanifar, Nature Physics **17**, 931 (2021), 2004.07266.

[29] E. v. d. Berg, Z. K. Minev, A. Kandala, and K. Temme, arXiv:2201.09866 (2022).

[30] M. P. A. Fisher, V. Khemani, A. Nahum, and S. Vijay, “Random quantum circuits,” (2022).

[31] A. C. Potter and R. Vasseur, in *Entanglement in Spin Chains*, Quantum Science and Technology (Springer, 2022) pp. 211–249, arXiv:2111.08018.

[32] Y. Imry and S.-k. Ma, Phys. Rev. Lett. **35**, 1399 (1975).

[33] A. Nahum, J. Ruhman, S. Vijay, and J. Haah, Phys. Rev. X **7**, 031016 (2017).

[34] A. Nahum, S. Vijay, and J. Haah, Phys. Rev. X **8**, 021014 (2018).

[35] C. W. von Keyserlingk, T. Rakovszky, F. Pollmann, and S. L. Sondhi, Phys. Rev. X **8**, 021013 (2018).

[36] J. Sun, X. Yuan, T. Tsunoda, V. Vedral, S. C. Benjamin, and S. Endo, Phys. Rev. Appl. **15**, 034026 (2021).

[37] N. Lashkari, D. Stanford, M. Hastings, T. Osborne, and P. Hayden, J. High Energy Phys. **2013**, 22 (2013).

[38] S.-K. Jian, G. Bentsen, and B. Swingle, arXiv:2206.14205 (2022), 10.48550/arxiv.2206.14205.

[39] C.-M. Jian, Y.-Z. You, R. Vasseur, and A. W. W. Ludwig, Phys. Rev. B **101**, 104302 (2020).

[40] Y. Bao, S. Choi, and E. Altman, Phys. Rev. B **101**, 104301 (2020).

[41] A. M. Dalzell, N. Hunter-Jones, and F. G. S. L. Brandão, PRX Quantum **3**, 010333 (2022).

[42] A. M. Dalzell, N. Hunter-Jones, and F. G. S. L. Brandão, (2021), arXiv:2111.14907 [quant-ph].

[43] A. Deshpande, P. Niroula, O. Shtanko, A. V. Gorshkov, B. Fefferman, and M. J. Gullans, PRX Quantum **3**, 040329 (2022).

[44] X. Gao, M. Kalinowski, C.-N. Chou, M. D. Lukin, B. Barak, and S. Choi, arXiv:2112.01657 (2021), 10.48550/arxiv.2112.01657.

[45] D. P. DiVincenzo, D. W. Leung, and B. M. Terhal, IEEE Transactions on Information Theory **48**, 580 (2002-03).

[46] B. Skinner, J. Ruhman, and A. Nahum, Phys. Rev. X **9**, 031009 (2019).

[47] Y. Li, X. Chen, and M. P. A. Fisher, Phys. Rev. B **100**, 134306 (2019).

[48] S. Boixo, S. V. Isakov, V. N. Smelyanskiy, R. Babbush, N. Ding, Z. Jiang, M. J. Bremner, J. M. Martinis, and H. Neven, Nat. Phys. **14**, 595 (2018).

[49] F. Arute, K. Arya, R. Babbush, D. Bacon, J. C. Bardin, R. Barends, R. Biswas, S. Boixo, F. G. S. L. Brandao, D. A. Buell, B. Burkett, Y. Chen, Z. Chen, B. Chiaro, R. Collins, W. Courtney, A. Dunsworth, E. Farhi, B. Foxen, A. Fowler, C. Gidney, M. Giustina, R. Graff, K. Guerin, S. Habegger, M. P. Harrigan,

M. J. Hartmann, A. Ho, M. Hoffmann, T. Huang, T. S. Humble, S. V. Isakov, E. Jeffrey, Z. Jiang, D. Kafri, K. Kechedzhi, J. Kelly, P. V. Klimov, S. Knysh, A. Korotkov, F. Kostritsa, D. Landhuis, M. Lindmark, E. Lucero, D. Lyakh, S. Mandrà, J. R. McClean, M. McEwen, A. Megrant, X. Mi, K. Michelsen, M. Mohseni, J. Mutus, O. Naaman, M. Neeley, C. Neill, M. Y. Niu, E. Ostby, A. Petukhov, J. C. Platt, C. Quintana, E. G. Rieffel, P. Roushan, N. C. Rubin, D. Sank, K. J. Satzinger, V. Smelyanskiy, K. J. Sung, M. D. Trevithick, A. Vainsencher, B. Villalonga, T. White, Z. J. Yao, P. Yeh, A. Zalcman, H. Neven, and J. M. Martinis, *Nature* **574**, 505 (2019).

[50] A. Bouland, B. Fefferman, C. Nirke, and U. Vazirani, *Nat. Phys.* **15**, 159 (2019).

[51] R. Movassagh, (2019), arXiv:1909.06210 [cond-mat, physics:hep-th, physics:math-ph, physics:quant-ph].

[52] Y. Wu, W.-S. Bao, S. Cao, F. Chen, M.-C. Chen, X. Chen, T.-H. Chung, H. Deng, Y. Du, D. Fan, M. Gong, C. Guo, C. Guo, S. Guo, L. Han, L. Hong, H.-L. Huang, Y.-H. Huo, L. Li, N. Li, S. Li, Y. Li, F. Liang, C. Lin, J. Lin, H. Qian, D. Qiao, H. Rong, H. Su, L. Sun, L. Wang, S. Wang, D. Wu, Y. Wu, Y. Xu, K. Yan, W. Yang, Y. Yang, Y. Ye, J. Yin, C. Ying, J. Yu, C. Zha, C. Zhang, H. Zhang, K. Zhang, Y. Zhang, H. Zhao, Y. Zhao, L. Zhou, Q. Zhu, C.-Y. Lu, C.-Z. Peng, X. Zhu, and J.-W. Pan, *Phys. Rev. Lett.* **127**, 180501 (2021).

[53] Q. Zhu, S. Cao, F. Chen, M.-C. Chen, X. Chen, T.-H. Chung, H. Deng, Y. Du, D. Fan, M. Gong, C. Guo, C. Guo, S. Guo, L. Han, L. Hong, H.-L. Huang, Y.-H. Huo, L. Li, N. Li, S. Li, Y. Li, F. Liang, C. Lin, J. Lin, H. Qian, D. Qiao, H. Rong, H. Su, L. Sun, L. Wang, S. Wang, D. Wu, Y. Wu, Y. Xu, K. Yan, W. Yang, Y. Yang, Y. Ye, J. Yin, C. Ying, J. Yu, C. Zha, C. Zhang, H. Zhang, K. Zhang, Y. Zhang, H. Zhao, Y. Zhao, L. Zhou, C.-Y. Lu, C.-Z. Peng, X. Zhu, and J.-W. Pan, arXiv:2109.03494 (2021), 10.48550/arxiv.2109.03494.

[54] S. Aaronson and S. Gunn, arXiv (2019), 10.48550/arxiv.1910.12085, arXiv:1910.12085.

[55] A. Bouland, B. Fefferman, Z. Landau, and Y. Liu, (2021), arXiv:2102.01738 [quant-ph].

[56] R. Movassagh, (2018), arXiv:1810.04681 [cond-mat, physics:hep-th, physics:math-ph, physics:quant-ph].

[57] D. Hangleiter and J. Eisert, arXiv:2206.04079 (2022), 10.48550/arxiv.2206.04079.

[58] X. Gao and L. Duan, (2018), arXiv:1810.03176 [quant-ph].

[59] D. Aharonov, X. Gao, Z. Landau, Y. Liu, and U. Vazirani, arXiv:2211.03999 (2022), 10.48550/arxiv.2211.03999.

Appendix A: Mean-Field Theory in Brownian Circuits

Here, we develop a mean-field theory for the error mitigation threshold in the noisy-mitigated Brownian circuit model.

The unitary dynamics in the Brownian quantum circuit model is described by a stochastic Hamiltonian

$$H(t) = \sum_{i < j, \mu, \nu} J_{ij\mu\nu}(t) \sigma_i^\mu \sigma_j^\nu, \quad (\text{A1})$$

where σ_i^μ are Pauli operators $\mu \in \{X, Y, Z\}$ for site i of N qubits and $J_{ij\mu\nu}(t)$ is a white-noise correlated coupling with variance [37, 38]

$$\langle J_{ij\mu\nu}(t) J_{kl\gamma\delta}(t') \rangle = \frac{J}{2N} \delta_{ik} \delta_{jl} \delta_{\mu\gamma} \delta_{\nu\delta} \delta(t - t'). \quad (\text{A2})$$

The noise and antinoise are treated using a Lindblad master equation

$$\dot{\rho} = -i[H(t), \rho] + \sum_i \frac{\gamma_i - \gamma_a}{4} \left(-3\rho + \sum_\mu \sigma_i^\mu \rho \sigma_i^\mu \right), \quad (\text{A3})$$

where γ_i is the local random noise rate and γ_a is the antinoise rate.

To analyze the dynamics we derive an effective master equation that describes the replicated system

$$M_k(\rho) = \mathbb{E}[U^{\otimes k} \rho U^{\dagger \otimes k}], \quad (\text{A4})$$

where $U = \mathcal{T} e^{-i \int_0^t dt' H(t')}$ is the time evolution operator under the Hamiltonian. Expanding to second order in an infinitesimal time-step, we arrive at the equation $M_k(\rho) = e^{\mathcal{L}_k t}$ for a Lindbladian \mathcal{L}_k given by

$$\mathcal{L}_k(\rho) = \frac{J}{2N} \sum_{i \neq j, \mu, \nu, r, s} \sigma_{ir}^\mu \sigma_{jr}^\nu \rho \sigma_{is}^\mu \sigma_{js}^\nu - \frac{1}{2} \{ \sigma_{ir}^\mu \sigma_{is}^\mu \sigma_{jr}^\nu \sigma_{js}^\nu, \rho \}, \quad (\text{A5})$$

where r and s are replica indices that run over $1, \dots, k$. Thus, we arrive at a master equation describing the average dynamics of the replicated density matrices

$$\dot{\rho} = \mathcal{L}_k(\rho) + \sum_i \frac{\gamma_i - \gamma_a}{4} \left(-3k\rho + \sum_{r, \mu} \sigma_{ir}^\mu \rho \sigma_{ir}^\mu \right). \quad (\text{A6})$$

To develop the mean field theory, we study the two-replica problem $k = 2$. Similar to a Haar random circuit, the Lindbladian \mathcal{L}_2 has two steady states $I^{\otimes N}$ and $S^{\otimes N}$. As our mean-field ansatz, we therefore use a product state of the form $\rho = \bigotimes_{i=1}^N \rho_i$. A further simplification arises from the nature of the dynamics that has an effective SU(2) symmetry in the average-replica dynamics. As a result, we can express

$$\rho_i = (1/4 + \delta_i) |s\rangle \langle s| + (1/4 - \delta_i/3) P_T, \quad (\text{A7})$$

where δ_i is the deviation from an infinite temperature state, $|s\rangle$ is a two-qubit singlet state across the two replicas, and P_T is the projector onto the two-qubit triplet subspace of the two replicas.

The mean-field equations for δ_i take the form

$$\dot{\delta}_i = -4 \left[\Delta_i + \frac{J}{N} \sum_{j \neq i} (3 + 4\delta_j) \right] \delta_i, \quad (\text{A8})$$

where $\Delta_i = \gamma_i - \gamma_a$. This equation has the two steady-state solutions $\delta_i = 0$ and $\delta_i = -3/4$, corresponding to the $I^{\otimes N}$ and $S^{\otimes N}$ solutions, respectively. In the case of binary disorder, we define two populations of sites $A_{1/2}$

such that $\Delta_i = \gamma_{1/2} - \gamma_a$, respectively, for $i \in A_{1/2}$. We have the zero-mean field condition $p\Delta_1 + (1-p)\Delta_2 = 0$. Defining $G_{\pm} = \frac{1}{N} \left(\sum_{i \in A_2} \delta_i \pm \sum_{i \in A_1} \delta_i \right)$, we arrive at simple closed set of equations in the large- N limit

$$\dot{G}_+ = -4J(3 + 4G_+)G_+ + \frac{4|\Delta_1|}{2(1-p)}[G_- - (2p-1)G_+],$$

$$\dot{G}_- = -4J(3 + 4G_-)G_- + \frac{4|\Delta_1|}{2(1-p)}[G_+ - (2p-1)G_-].$$

Setting $p = 1/2$, these equations reduce to the particularly simple form

$$\dot{G}_+ = -4J(3 + 4G_+)G_+ + 4|\Delta_1|G_-, \quad (\text{A9})$$

$$\dot{G}_- = -4J(3 + 4G_-)G_- + 4|\Delta_1|G_+, \quad (\text{A10})$$

For general p , the steady state solutions are $G_+ = 0, -(3 - |\Delta_1|/J)/4, -(3 + \Delta_2/J)/4$. The all identity solution $G_+ = G_- = 0$ only becomes an unstable fixed point for $|\Delta_1|/J \geq 3$, whereas it remains stable for weaker disorder. As a result, the phase transition in the mean-field theory occurs at the disorder strength $|\Delta_1| = 3J$. Beyond this value of disorder, the mean-field steady-state solution flows to an unphysical state; however, for weaker disorder, the physical mean-field solution remains stable.

Appendix B: Statistical Mechanics Mapping Formalism

Here, we review the statistical mechanics for the model with noise and antinoise, generalizing the mappings studied in Ref. [34, 39–42]. In this paper, we focus our attention to calculating second-moment quantities of a quantum state, which includes measures like fidelity, collision probability, and linear cross entropy. The circuit-averaged calculations of such quantities lends itself to a statistical mechanical mapping to an Ising spin model.

Consider a second moment measure M , averaged over circuits from ensemble \mathcal{U} . For a state ρ_C of dimension $2^{2n} \times 2^{2n}$, generated using a circuit C from an ensemble \mathcal{U} , a circuit-averaged second moment measure M for ρ_C can be written as a two-copy expectation of a linear operator O_M of dimension $2^{4n} \times 2^{4n}$.

$$\begin{aligned} \mathbb{E}_{C \in \mathcal{U}}[M[\rho_C]] &= \mathbb{E}_{C \in \mathcal{U}}[\text{tr}(O_M \rho_C \otimes \rho_C)] \\ &= \text{tr}(O_M \mathbb{E}_{C \in \mathcal{U}}[\rho_C \otimes \rho_C]) \end{aligned} \quad (\text{B1})$$

The circuit-averaged two-copy state $\mathbb{E}_{C \in \mathcal{U}}[\rho_C \otimes \rho_C]$, therefore, enables us to calculate second-moment measures.

We consider circuit models that can be decomposed into a series of elementary two-qubit gates (noisy or noiseless), each drawn independently from the two-qubit Haar ensemble \mathcal{U}_2 . The action of the circuit map on two-copies of an initial input state is, thus, given by

$$\rho_C \otimes 2 = C_s \circ C_{s-1} \circ \dots \circ C_1[\rho_0 \otimes \rho_0], \quad (\text{B2})$$

where the elementary single-qubit or two-qubit channels are indexed using integers $[1, s]$. For noiseless gates, $C_i[\rho_0 \otimes \rho_0] = (C_i \otimes C_i)\rho(C_i^\dagger \otimes C_i^\dagger)$. We can model a noisy circuit by adding error channel \mathcal{E} after each noiseless gate:

$$\rho_C^{\otimes 2} = \mathcal{E}_s \circ C_{s-1} \circ \mathcal{E}_{s-1} C_{s-1} \circ \dots \circ \mathcal{E}_1 \circ C_1[\rho_0 \otimes \rho_0]. \quad (\text{B3})$$

In general, the error channel may act on any set of qubits. For our purposes, we assume that the error channel \mathcal{E}_i acts on the qubit or the pair of qubits acted on by the noiseless gate C_i . Since we draw each gate from the random one-qubit or two-qubit Haar ensemble, we can replace the noiseless maps $C_i[\rho]$ with the gate-averaged map $\bar{C}_i[\sigma] = \mathbb{E}_{C \in \mathcal{U}_{1/2}} C[\sigma]$,

$$\mathbb{E}_{C \in \mathcal{U}}[\rho_C \otimes \rho_C] = \mathcal{E}_s \circ \bar{C}_{s-1} \circ \mathcal{E}_{s-1} \bar{C}_{s-1} \circ \dots \circ \mathcal{E}_1 \circ \bar{C}_1[\rho_0 \otimes \rho_0]. \quad (\text{B4})$$

The action of a random single-qubit gate C , on a state residing in the two-copy Hilbert space is given by

$$\bar{C}^{(1)}[\sigma] = \frac{\text{tr}((1 - S/2)\sigma)}{3} I + \frac{\text{tr}((S - 1/2)\sigma)}{3} S, \quad (\text{B5})$$

where I and S are the 4×4 identity matrix and SWAP matrices, respectively. Similarly, the action of a random two-qubit gate on two copies of a qubit-pair is given by

$$\bar{C}^{(2)}[\sigma] = \frac{\text{tr}((1 - SS/4)\sigma)}{15} II + \frac{\text{tr}((SS - 1/4)\sigma)}{15} SS, \quad (\text{B6})$$

where we use the shorthand $SS = S \otimes S$ and $II = I \otimes I$. If two copies of a quantum state can be represented by a string of $\rho^{\otimes 2} \in \{I, S\}^n$, a single-qubit gate acts on qubit k by modifying the j th bit of the I-S string using the transition rules

$$I \rightarrow I \quad S \rightarrow S, \quad (\text{B7})$$

while leaving the rest of the bits in the string unchanged. Similarly, a two-qubit gate acting on qubits j and k modifies the j th and k th bits according to the transition rules:

$$II \rightarrow II \quad IS, SI \rightarrow \frac{2}{5}(II + SS) \quad SS \rightarrow SS. \quad (\text{B8})$$

A noiseless random circuit, therefore, can be represented as a linear operator acting on the reduced space spanned by basis elements in $\{I, S\}^n$, with each noiseless single-qubit gate given an identity map, and a two-qubit gate given by the transition matrix

$$T[\bar{C}^{(2)}] = \begin{pmatrix} 1 & 2/5 & 2/5 & 0 \\ 0 & 0 & 0 & 0 \\ 0 & 0 & 0 & 0 \\ 0 & 2/5 & 2/5 & 1 \end{pmatrix}. \quad (\text{B9})$$

We can similarly, find the transition matrices corresponding to the noise and antinoise channel. The single-qubit depolarization channel with error rate q , given by the following map

$$\mathcal{E}^{(1)}(\rho) = (1 - q)\rho + q \text{tr}(\rho) \frac{1}{2}, \quad (\text{B10})$$

acts on two copies of a qubit such that

$$\mathcal{E}[I] = \mathcal{E}[I_2 \otimes I_2] = \mathcal{E}^{(1)}[I_2] \otimes \mathcal{E}^{(1)}[I_2] = I_2 \otimes I_2 = I \quad (\text{B11})$$

, where I_2 is a 2×2 identity matrix. Similarly,

$$\begin{aligned} \mathcal{E}[S] &= (\mathcal{E}^{(1)} \otimes \mathcal{E})[I_2 \otimes I_2 + X \otimes X + Y \otimes Y + Z \otimes Z]/2 \\ &= [I_2 \otimes I_2 + (1-q)^2 (X \otimes X + Y \otimes Y + Z \otimes Z)]/2 \\ &= [(1 - (1-q)^2)/2I + (1-q)^2 S] \end{aligned}$$

where we have used the fact that $S = (I_2 \otimes I_2 + X \otimes X + Y \otimes Y + Z \otimes Z)/2$. The transition matrix corresponding to a depolarizing noise, in the statistical mechanical picture is given by,

$$T[\mathcal{E}_q] = \begin{pmatrix} 1 & (1 - (1-q)^2)/2 \\ 0 & (1-q)^2 \end{pmatrix} \quad (\text{B12})$$

Likewise, the antinoise channel of strength q_a , given by

$$\mathcal{A}^{(1)}(\rho) = \frac{1}{1-q_a} \left(\rho - q_a \text{tr}(\rho) \frac{1}{2} \right), \quad (\text{B13})$$

acts on two-copies of a qubit such that

$$\mathcal{A}[I] = (\mathcal{A}^{(1)} \otimes \mathcal{A}^{(1)})[I_2 \otimes I_2] = I, \text{ and} \quad (\text{B14})$$

$$\mathcal{A}[S] = \left[\left(1 - \frac{1}{(1-q_a)^2} \right) \frac{I}{2} + \frac{1}{(1-q_a)^2} S \right], \quad (\text{B15})$$

giving a transition matrix

$$T[\mathcal{A}_{q_a}] = \begin{pmatrix} 1 & (1 - (1-q_a)^{-2})/2 \\ 0 & (1-q_a)^{-2} \end{pmatrix} \quad (\text{B16})$$

Concatenating the transition matrix for the noise channel and the antinoise channel gives the transition matrix for the composite channel. $T[\mathcal{A}_{q_a} \circ \mathcal{E}_q] = T[\mathcal{A}_{q_a}] \cdot T[\mathcal{E}_q]$.

In our simulations, we start with an initial state drawn from the Haar ensemble or a random product state. A Haar random state is proportional to $I^{\otimes n} + S^{\otimes n}$ in the two-copy description, while a random product state is proportional to $(I + S)^{\otimes n}$. We can then use the statistical mechanical formalism discussed above to evolve this state using the respective transition matrices for two-qubit gates, noise and antinoise channels.

Appendix C: Local Probe

In Fig. 2, we presented different correlation metrics between two qubits in the system as a probe of the phase transition. Here, we present an alternative metric based on the entropy of a single qubit in the system.

Deep in the below threshold phase, this single-qubit entropy quantity saturates to one bit, while above threshold it diverges to large negative values due to the unphysical density matrix. As a result, we expect a crossing to occur at the phase transition. Numerical simulations

of the two-replica stat-mech model for the all-to-all circuit model illustrate this behavior. In Fig. 3(a), we show the unscaled behavior of the entropy for different system sizes, which shows a crossing near $\sigma_c/\bar{q} = 0.65(5)$. Collapsing the data with this value of σ_c fixed, we estimate a critical exponent $\mu = 1.0(2)$. In Fig. 2(c-d), we fixed $\mu = 1$ in collapsing the mutual information data based on these scaling results. This single-qubit quantity also has advantages for experimental probes of the transition as it requires minimal tomographic overhead to estimate.

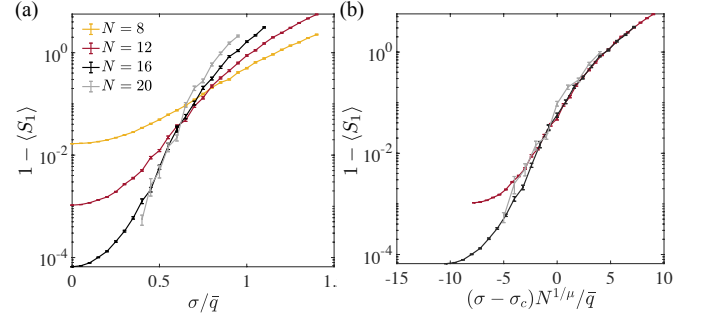


FIG. 3. Local probe of the error mitigation threshold: (a) Entanglement entropy of a single-site in the system for different system sizes. The larger sizes begin to develop a crossing, indicative of the phase transition. (b) Scaling collapse for $\sigma_c/\bar{q} = 0.65(5)$ and $\mu = 1.0(2)$.

Appendix D: Error Mitigated Fidelity Benchmarks

Here, we introduce mitigated fidelity benchmarks and demonstrate an exponential improvement in a mitigated version of the linear cross-entropy benchmark below the error mitigation threshold.

The task of sampling from the output distribution of a noiseless random circuit is widely conjectured to be intractable with classical computers [48, 50, 56, 57]. This conjecture forms the basis for claims of achievement of quantum computational advantage in recent experiments [49, 52, 53]. The experimental claims remain controversial, however, partly because of the effects of noise on the output that render the signal classically simulatable at high depth [55, 58, 59]. To provide evidence that the output signal still remains close to the ideal case, one can estimate fidelity benchmarks using the samples from the experiment. Verifying the claim of computational advantage in the case of noisy circuits then reduces to the task of achieving a sufficiently high “score” on the benchmark [54].

Recall that the linear XEB is given by the formula

$$F_{\text{XEB}} = 2^n \sum_x p_n(x) p_0(x) - 1, \quad (\text{D1})$$

where $p_0(x) = |\langle x | U_d \cdots U_1 | 0 \rangle|^2$ is the probability of measuring outcome x for the noiseless circuit of depth d and

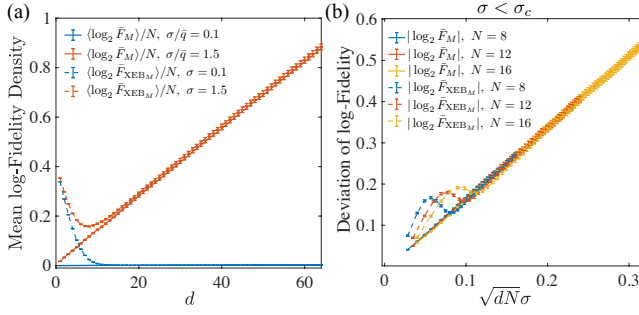


FIG. 4. Dynamics of fidelity benchmarks above and below threshold: (a) Disorder-averaged mean value of the logarithm of the circuit averaged mitigated fidelity $-\langle \log \bar{F}_M \rangle / N$ and cross-entropy benchmarking mitigated fidelity $-\langle \log \bar{F}_{XEB_M} \rangle / N$ above and below the error mitigation threshold in the all-to-all model. (b) Dynamics of the standard deviation over the noise of the log-circuit-averaged mitigated fidelities below threshold showing the improved scaling of the typical log-fidelity as $\pm \mathcal{O}(\sqrt{Nd})$.

$p_n(x) = \langle x | \mathcal{A} \circ \mathcal{U}_d \circ \dots \circ \mathcal{E}_1 \circ \mathcal{U}_1 (|0\rangle\langle 0|) | x \rangle$ is the analogous probability for the noisy circuit.

We now introduce the mitigated linear XEB, which is instead given by the formula

$$F_{XEB_M} = 2^n \sum_x p_n(x) p_a(x) - 1, \quad (D2)$$

where $p_a(x) = \langle x | \mathcal{A} \circ \mathcal{U}_d \circ \dots \circ \mathcal{A} \circ \mathcal{U}_1 (|0\rangle\langle 0|) | x \rangle$ is a quasi-probability for the circuit with antinoise inserted in place of noise. The quantity $p_a(x)$ can be computed on a classical computer, which leads to a sampling formula for F_{XEB_M} using M samples x_i obtained from $p_n(x)$

$$F_{XEB_M} = \frac{2^n}{M} \sum_{i=1}^M p_a(x_i) - 1. \quad (D3)$$

This formula illustrates that the mitigated fidelity can be obtained without directly implementing PEC except in purely classical post-processing. After circuit averaging, one can quickly show that for depolarizing noise and its antinoise partner, the mitigated fidelity is equivalent to the formula

$$\bar{F}_{XEB_M} = 2^n \sum_x p_0(x) p_{an}(x) - 1, \quad (D4)$$

where $p_{an}(x) = \langle x | \mathcal{A} \circ \mathcal{E}_d \circ \mathcal{U}_d \circ \dots \circ \mathcal{A} \circ \mathcal{E}_1 \circ \mathcal{U}_1 (|0\rangle\langle 0|) | x \rangle$ implements the antinoise on the same copy as the noise. This identity follows because the noise and antinoise on one copy have the identical effect on the I and S operators after averaging over circuits. From this expression, we see that, in the case of perfect mitigation, \bar{F}_{XEB_M} reduces to its ideal value.

We can also define a mitigated fidelity that takes the form

$$F_M = \text{tr}[\mathcal{A} \circ \mathcal{U}_d \circ \dots \circ \mathcal{A} \circ \mathcal{U}_1 (|0\rangle\langle 0|) \times \mathcal{E}_d \circ \mathcal{U}_d \circ \dots \circ \mathcal{E}_1 \circ \mathcal{U}_1 (|0\rangle\langle 0|)].$$

In the case where $\mathcal{E}_i = \mathcal{A}^{-1}$ for every i , we can see that $F_M = 1$.

In Fig. 4], we show that the log-fidelity at low noise rates and d grows as $\mathcal{O}(Nd)$, whereas using error mitigation this scaling can be improved to $\mathcal{O}(\sqrt{Nd})$, representing an exponential improvement in the score that brings it closer to the $\mathcal{O}(d)$ scaling of the log-total variation distance [43]. Moreover, as explained above, the cross-entropy benchmark fidelity can be mitigated entirely in classical post-processing. As a result, the mitigated XEB fidelity can be estimated with existing experimental data from random circuit sampling experiments.